Hysteresis in the gait transition of a quadruped investigated using simple body mechanical and oscillator network models

Shinya Aoi,[1,3] Tsuyoshi Yamashita,[1] and Kazuo Tsuchiya[2,3]

[1]*Deptartment of Aeronautics and Astronautics, Graduate School of Engineering, Kyoto University,*
Yoshida honmachi, Sakyo-ku, Kyoto 606-8501, Japan
[2]*Department of Energy and Mechanical Engineering, Faculty of Science and Engineering, Doshisha University,*
1-3 Tatara, Miyakodani, Kyotanabe, Kyoto 610-0394, Japan
[3]*JST, CREST, 5 Sanbancho, Chiyoda-ku, Tokyo 102-0075, Japan*

We investigated the dynamics of quadrupedal locomotion by constructing a simple quadruped model that consists of a body mechanical model and an oscillator network model. The quadruped model has front and rear bodies connected by a waist joint with a torsional spring and damper system and four limbs controlled by command signals from the oscillator network model. The simulation results reveal that the quadruped model produces various gait patterns through dynamic interactions among the body mechanical system, the oscillator network system, and the environment. They also show that it undergoes a gait transition induced by changes in the waist joint stiffness and the walking speed. In addition, the gait pattern transition exhibits a hysteresis similar to that observed in human and animal locomotion. We examined the hysteresis mechanism from a dynamic viewpoint.

I. INTRODUCTION

Humans and animals perform adaptive walking in diverse environments by cooperatively and skillfully manipulating their complicated and redundant musculoskeletal systems. A characteristic of adaptive walking is that the gait pattern varies depending on the locomotion speed (e.g., humans walk and run, and quadrupeds walk, trot, and gallop). Experimental studies have revealed that there is a hysteresis associated with changes in the gait pattern; in other words, the gait transition occurs at different locomotion speeds depending on the speed change direction [1–8]. Gait transitions have been investigated from mechanical, energetic, kinematic, and kinetic viewpoints [2,6,8–10]; however, it is still unclear what determines gait transitions.

The ability of animals to perform adaptive movements has been investigated by examining the configurations and activities of neural systems. For example, neurophysiological studies using lampreys and decerebrate cats have greatly contributed to elucidating locomotor mechanisms in animals [11–14]. Various neural network models have been developed that represent gait patterns in terms of the phase relationship between the limb movements [15–19]. However, it is difficult to fully analyze locomotion mechanisms solely in terms of the nervous system because locomotion is a well-organized motion generated through dynamic interactions among the body, the nervous system, and the environment. In addition to analyzing the nervous system, it is crucial to elucidate the inherent dynamic characteristics of the body. Studies of the nervous and musculoskeletal systems must complement each other in order to clarify locomotion mechanisms.

To investigate the dynamic characteristics of the body mechanical system and the functional roles of the nervous system, various simple models have recently been developed by extracting the fundamentals of locomotion dynamics for humans [20–28] and animals [29–35]. In the present study we constructed a simple quadruped model by employing a body mechanical model for the musculoskeletal system and an oscillator network model for the nervous system to emulate dynamic locomotion of quadrupeds. We performed numerical simulations and examined the dynamic characteristics of quadrupedal locomotion. We particularly focused on the effect of locomotion speed and waist joint stiffness on gait patterns. The simulation results reveal that the quadruped model creates various gait patterns through dynamic interactions among the body dynamics, the oscillator dynamics, and the environment. They also show that gait transitions occur due to changes in the locomotion speed and the waist joint stiffness of the quadruped. In addition, gait transitions in the model exhibit a hysteresis similar to that observed in humans and animals. We investigated the dynamic characteristics of this hysteresis.

II. METHODS

A. Body mechanical model

Figure 1 shows the body mechanical model of our quadruped model, which consists of two rigid bodies and four limbs. Each limb consists of two rigid links connected by pitch joints. The two rigid bodies are connected to each other by a roll joint (waist joint). Limb joint movements are actively generated by motor commands, whereas the waist joint moves passively through an inherent torsional spring and damper system. Ankles are neglected and no torque is generated between the limb tips and the ground.

The limbs are enumerated limbs 1 to 4, and the limb joints are numbered joints 1 and 2. To describe the configuration of this model, we describe the position of the center of mass of the front body by x_1, x_2, and x_3, and the Euler angles that express the posture of the front body by θ_1, θ_2, and θ_3. We denote the rotation angle of joint j of limb i by θ_j^i ($i = 1, \ldots, 4$, $j = 1, 2$) and the waist joint angle by θ_w.
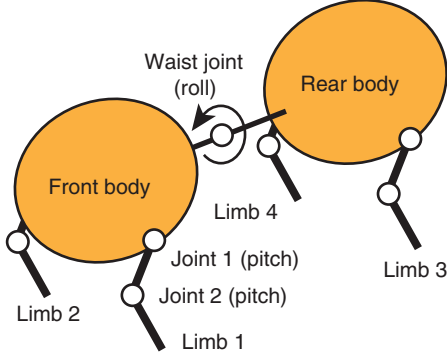
FIG. 1. (Color online) Body mechanical model of quadruped model consisting of two bodies and four limbs.

For the state variable $q = [\, x_i \; \theta_i \; \theta_w \; \theta_k^j \,]^T \in \mathbb{R}^{15}$ ($i = 1,2,3$, $j = 1,\ldots,4$, $k = 1,2$), the equation of motion of this body mechanical model is expressed by Lagrangian equations as

$$K(q)\ddot{q} + h(q,\dot{q}) = v(q) + u(q,\dot{q}) + \lambda(q,\dot{q}), \qquad (1)$$

where $K(q) \in \mathbb{R}^{15 \times 15}$ is the inertia matrix, $h(q,\dot{q}) \in \mathbb{R}^{15}$ is the nonlinear term that includes Coriolis and centrifugal forces, $v(q) \in \mathbb{R}^{15}$ is the gravity term, $u(q,\dot{q}) \in \mathbb{R}^{15}$ is the joint torque term, and $\lambda(q,\dot{q}) \in \mathbb{R}^{15}$ is the reaction force from the ground (see Appendix). We used viscoelastic elements to model the contact between the limb tips and the ground. The limb tips rarely slip since we employed large values for the viscoelastic parameters. We performed forward dynamic simulations by solving the equation of motion using the fourth-order Runge–Kutta method with a step size of 0.1 ms. Table I shows the physical parameters of the quadruped model; the two bodies had the same parameter values as each other, and the four limbs also had the same parameter values as each other.

B. Oscillator network model

In humans and animals, motor commands are generated by integrating input from higher centers and afferent feedback in the spinal cord. These commands produce muscle activity that moves the skeletal system. Physiological studies suggest that central pattern generators (CPGs) in the spinal cord strongly contribute to rhythmic limb movement such as locomotion [11,13,14]. The organization of CPGs remains unclear. Various CPG models have been proposed, such as the half-center model and the unit burst generator model [36,37]. However, recent neurophysiological findings suggest that CPGs consist of hierarchical networks that include rhythm generator (RG)

TABLE I. Physical parameters of the quadruped model

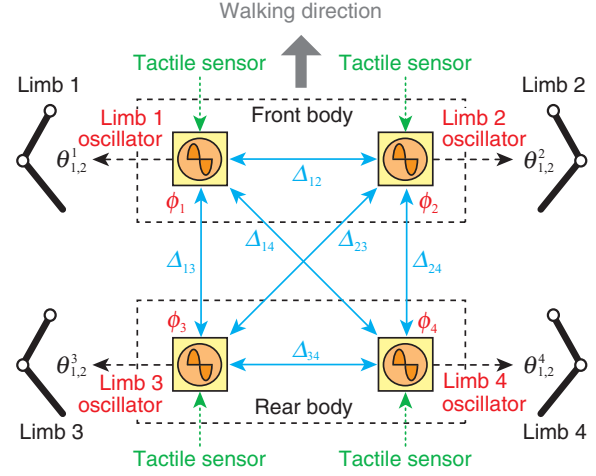| Link	Parameter	Value
Body	Mass [kg]	1.0
	Length [cm]	10.0
	Width [cm]	10.0
Upper limb	Mass [kg]	0.1
	Length [cm]	8.0
Lower limb	Mass [kg]	0.1
	Length [cm]	8.0

FIG. 2. (Color online) Oscillator network model with four oscillators. Solid blue arrows indicate interactions among the oscillators based on the phase relationship Δ_{ij}. The oscillator phases are modulated by tactile sensor information (dotted green arrows). The oscillator phases determine the limb joint kinematics (dashed black arrows).

and pattern formation (PF) networks [38–41]. The RG network generates the basic rhythm and modifies it by producing phase shifts and rhythm resetting in response to sensory afferents and perturbations (phase resetting). The PF network shapes the rhythm into spatiotemporal patterns of muscle activation. CPGs control the locomotor rhythm in the RG network and the muscle activation pattern in the PF network independently.

In this paper we constructed an oscillator network model using four oscillators based on a two-layer hierarchical network model (Fig. 2). In this model the RG model produces rhythm information for locomotor behavior and regulates it in response to tactile sensory information based on a phase resetting mechanism. The PF model generates motor commands based on the rhythm information from the RG model to produce the limb movements. The following sections explain the details of the model.

1. Rhythm generator model

The RG model produces rhythm information for the locomotor behavior through interactions among the body mechanical system, the oscillator network system, and the environment. For the RG model, we used four simple phase oscillators (limb 1 . . . 4 oscillators), each of which generates a basic rhythm and phase information for the corresponding limb. We defined ϕ_i ($i = 1,\ldots,4$) as the phase of the limb i oscillator ($0 \leqslant \phi_i \leqslant 2\pi$) and employed the following phase dynamics:

$$\dot{\phi}_i = \omega + g_{1i} + g_{2i}, \quad i = 1,\ldots,4, \qquad (2)$$

where ω is the basic oscillator frequency, which has the same value for all four oscillators, g_{1i} ($i = 1,\ldots,4$) is the function for the gait pattern (see Sec. II B 3), and g_{2i} ($i = 1,\ldots,4$) is the function arising from the phase and rhythm modulation based on phase resetting in response to tactile sensory information (see Sec. II B 4).
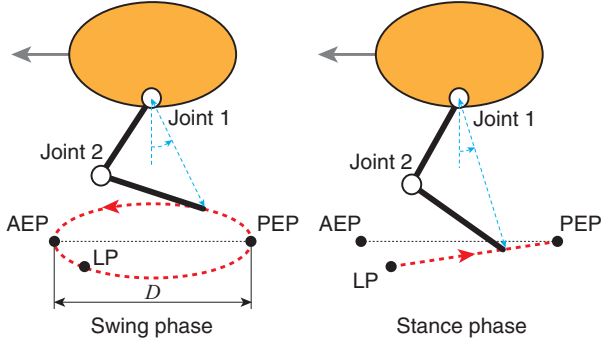
FIG. 3. (Color online) Limb joint kinematics composed of swing and stance phases, which were determined from the length and orientation of the limb axis. The kinematics changes from the swing to stance phase when the limb tip contacts the ground. When the limb tip reaches the PEP, it moves into swing phase.

2. Pattern formation model

The PF model generates motor commands based on the oscillator phase ϕ_i from the RG model to produce limb movement. Recent neurophysiological studies have revealed that spinocerebellar neurons receive sensory signals from proprioceptors and cutaneous receptors and encode the global parameters of the limb kinematics (namely, the length and orientation of the limb axis, which represents the position of the foot relative to the hip) [42–44]. In this study we used the PF model to generate motor commands to determine these global parameters of the limb kinematics.

Human and animal locomotion involves moving the center of mass forward without falling over. To achieve this, the swing limb is advanced. When the swing limb touches the ground, it supports the body and generates a propulsive force from the ground. For simplicity, in our model we used limb kinematics composed of swing and stance phases in the pitch plane relative to the body, which are determined by the length and orientation of the limb axis (Fig. 3). During the swing phase, the limb tip follows a simple closed curve that includes the anterior extreme position (AEP) and the posterior extreme position (PEP). This curve starts from the PEP and continues until the limb tip touches the ground. During the stance phase, the limb tip traces out a straight line from the landing position (LP) to the PEP. During this phase, the limb tip moves in the opposite direction to the body. The body travels in the walking direction while the limb tips are in contact with the ground.

For this limb movement, we used D to denote the distance between the AEP and the PEP. We defined the swing and stance phase durations as T_{sw} and T_{st}, respectively, for the case when the limb tip contacts the ground at the AEP (LP = AEP). The duty factor β (i.e., the ratio between the stance phase and the step cycle duration), the basic frequency ω in (2), the stride length S, and the locomotion speed v are then respectively given by

$$\beta = \frac{T_{st}}{T_{sw} + T_{st}}$$

$$\omega = \frac{2\pi}{T_{sw} + T_{st}}$$

$$S = \frac{T_{sw} + T_{st}}{T_{st}} D$$

$$v = \frac{D}{T_{st}}. \quad (3)$$

These values are satisfied regardless of the gait pattern. We used the same values of these parameters for the limbs, which allows the quadruped model to walk in a straight line and produce a single periodic gait. In the present study we used $D = 5.6$ cm and $T_{sw} = 0.1$ s, and we varied the locomotion speed v by changing the stance phase duration T_{st} in the same manner as humans and animals [45,46].

These two trajectories of the limb tip are given as functions of the corresponding oscillator phase, where we used $\phi_i = 0$ ($= 2\pi$) at the PEP and $\phi_i = \phi_{AEP}[= 2\pi(1 - \beta)]$ at the AEP. Consequently, the desired joint kinematics θ_j^{i*} ($i = 1, \ldots, 4$, $j = 1, 2$) for joint j of limb i is given as a function of the phase ϕ_i of the limb i oscillator and each limb joint is controlled by the joint torque based on proportional-derivative (PD) feedback control to produce the desired kinematics by

$$u_j^i = -\kappa_j^i\big(\theta_j^i - \theta_j^{i*}(\phi_i)\big) - \sigma_j^i\dot{\theta}_j^i, \quad i = 1, \ldots, 4, j = 1, 2, \quad (4)$$

where u_j^i ($i = 1, \ldots, 4$, $j = 1, 2$) is the torque at joint j of limb i and κ_j^i and σ_j^i ($i = 1, \ldots, 4$, $j = 1, 2$) are the gain constants.

3. Gait pattern

Since the limb kinematics is produced by the corresponding oscillator phase, the gait pattern is determined by the phase difference between the oscillators, which is given by the matrix Δ_{ij} ($0 \leqslant \Delta_{ij} \leqslant 2\pi$) as follows:

$$\Delta_{ij} = \phi_i - \phi_j, \quad i, j = 1, \ldots, 4. \quad (5)$$

For the phase difference, $\Delta_{ij} = -\Delta_{ji}$, $\Delta_{ij} = \Delta_{ik} + \Delta_{kj}$, and $\Delta_{ii} = 0$ ($i, j, k = 1, \ldots, 4$) are satisfied, and the gait pattern is determined by three state variables, such as $[\,\Delta_{12}\ \Delta_{13}\ \Delta_{34}\,]$. For example, $[\,\Delta_{12}\ \Delta_{13}\ \Delta_{34}\,] = [\,\pi\ \pi/2\ \pi\,]$ is satisfied for the walk pattern, in which the four limbs are not synchronized, $[\,\Delta_{12}\ \Delta_{13}\ \Delta_{34}\,] = [\,\pi\ \pi\ \pi\,]$ is satisfied for the trot pattern, in which the right and left limbs move out of phase and a forelimb and the contralateral hindlimb move in phase, and $[\,\Delta_{12}\ \Delta_{13}\ \Delta_{34}\,] = [\,\pi\ 0\ \pi\,]$ is satisfied for the pace pattern, in which the right and left limbs move out of phase and the ipsilateral limbs move in phase (Fig. 4).

Function g_{1i} in the phase dynamics (2) manipulates the phase difference between the oscillators for the gait pattern. It is given by

$$g_{1i} = -\sum_{j=1}^{4} K_{ij} \sin\big(\phi_i - \phi_j - \Delta_{ij}^*\big), \quad i = 1, \ldots, 4, \quad (6)$$

where Δ_{ij}^* is the desired phase difference and K_{ij} ($i, j = 1, \ldots, 4$) is the gain constant ($K_{ij} \geqslant 0$). This type of function is widely employed for interactions in oscillator network systems [19,47–55]. When a large value is used for K_{ij}, $\phi_i - \phi_j = \Delta_{ij}^*$ ($\Delta_{ij} = \Delta_{ij}^*$) is satisfied. The solid blue arrows in Fig. 2 indicate these interactions among the oscillators.
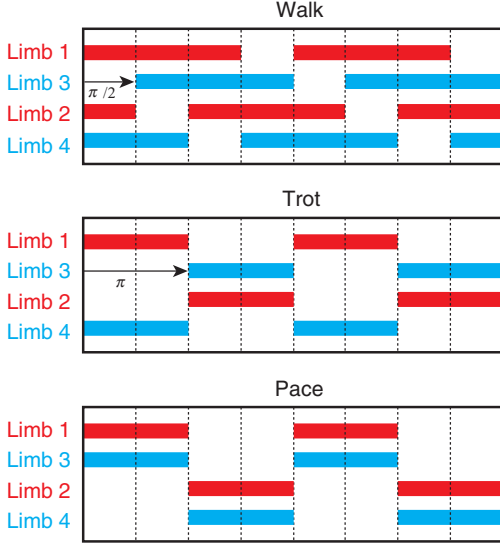
FIG. 4. (Color online) Footprint diagrams for walk, trot, and pace patterns in which the right and left limbs move out of phase [red: forelimbs (limbs 1 and 2); blue: hindlimbs (limbs 3 and 4)].

4. Phase resetting

The CPGs can produce oscillatory behaviors even in the absence of rhythmic input and proprioceptive feedback. However, they have to employ sensory feedback to produce adaptive and effective locomotor behavior. Physiological findings suggest that the locomotor rhythm generated by the CPGs is modulated by phase resetting in response to sensory afferent or perturbations [39,40,56,57]. The functional roles of phase resetting in the generation of adaptive walking have been investigated using neuromusculoskeletal models [21,58]. To create adaptive locomotor behavior of our quadruped model through dynamic interactions among the body mechanical system, the oscillator network system, and the environment, we modulated the locomotor phase and rhythm by phase resetting in response to tactile sensory information.

Function g_{2i} in (2) corresponds to this modulation due to phase resetting. When the tip of limb i lands on the ground, the phase ϕ_i of the limb i oscillator is reset to ϕ_{AEP} from ϕ_{land}^i at the landing ($i = 1, \ldots, 4$). Therefore, function g_{2i} is written as

$$g_{2i} = \left(\phi_{\text{AEP}} - \phi_{\text{land}}^i\right)\delta\left(t - t_{\text{land}}^i\right), \quad i = 1, \ldots, 4 \quad (7)$$

where t_{land}^i is the time when the tip of limb i contacts the ground ($i = 1, \ldots, 4$) and $\delta(\cdot)$ denotes Dirac's δ function. Note that tactile sensor signals not only modulate the locomotion phase and rhythm, but also change the limb movements from the swing to the stance phase, as described in Sec. II B 2.

C. Waist joint stiffness

In our model the waist joint moves passively based on a torsional spring and damper system (unlike the limb joints that actively move in response to motor commands). We denote the spring constant as κ_{w} and the damping constant as σ_{w} (see Appendix). In animal locomotion, the gait transition is

affected by not only locomotion speed but also by physical conditions (e.g., carrying a weight) [10]. In this study, in addition to the walking speed, we examined the role of the waist joint stiffness on the locomotion of our quadruped model. We changed constants κ_{w} and σ_{w} using parameter f as follows:

$$\kappa_{\text{w}} = \kappa_0 (2\pi f)^2, \quad \sigma_{\text{w}} = 2\kappa_0 \zeta_0 (2\pi f), \quad (8)$$

where κ_0 and ζ_0 are constants, and we used $\zeta_0 = 1.0$ to provide adequate damping for the change in the waist joint stiffness by parameter f [59].

D. Constraints for gait pattern

During locomotion, the gait pattern is determined by the phase relationship between the oscillators, which is produced by interactions among the oscillators (6) and phase regulation by phase resetting (7). When we use neither (6) nor (7), the phase relationship remains that of the initial state and the gait pattern does not change. When all the elements of the desired phase relationship Δ_{ij}^* are given based on the desired gait pattern and large gain constants K_{ij} are used in (6), the quadruped model produces the desired gait pattern when the gait pattern is stable. In contrast, when small gain constants K_{ij} are used, the quadruped model may produce a different gait pattern from the desired one due to phase regulation by phase resetting (7) through locomotion dynamics.

We focused on the gait pattern in which the right and left limbs in each body move out of phase with each other. That is, we used

$$\Delta_{12}^* = \Delta_{34}^* = \pi \quad (9)$$

and large gain constants K_{12}, K_{21}, K_{34}, and K_{43}. Therefore, $\Delta_{12} = \Delta_{34} = \pi$ is generally satisfied, meaning that there are two constraints on the gait pattern. In contrast, we set the other gain constants K_{ij} to zero, so that the phase relationship between the forelimbs and hindlimbs, such as Δ_{13}, had no constraint and were solely determined by the locomotion dynamics. Under these conditions, the gait pattern is determined by a single phase relationship, such as Δ_{13}, which will be obtained through dynamic interactions among the body mechanical system, the oscillator network system, and the environment. For example, the quadruped model performs the walk pattern when $\Delta_{13} = \pi/2$, the trot pattern when $\Delta_{13} = \pi$, and the pace pattern when $\Delta_{13} = 0$ (Fig. 4).

III. RESULTS

A. Emergence of hysteresis in gait transition

1. Hysteresis by varying the waist joint stiffness

To investigate the effects of the waist joint stiffness on locomotor behavior, we conducted numerical simulations based on parameter f in (8). Specifically, we slowly increased the stride length from 0 (standing posture) to S to establish stable locomotion and used various initial values for the phase difference Δ_{13} with $f = 2.0$ or $f = 3.2$. After the quadruped model established a steady gait pattern, we slowly increased f
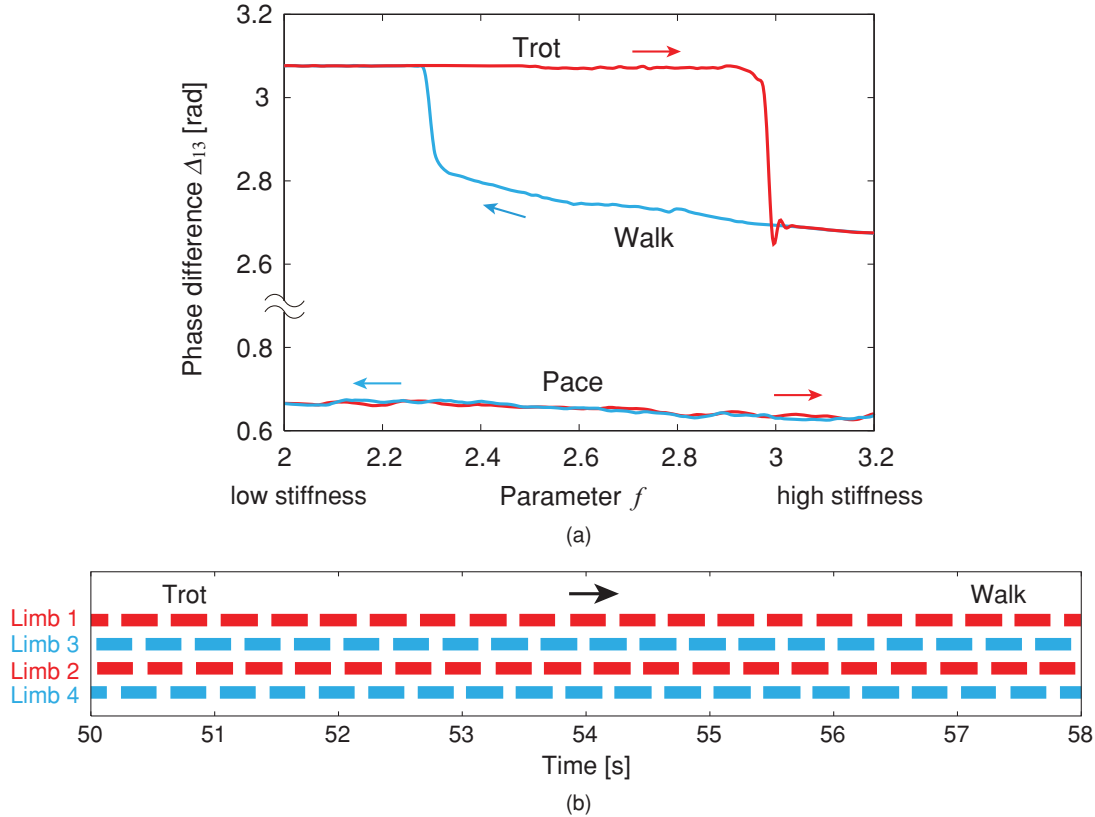
FIG. 5. (Color online) Gait transition induced by varying the waist joint stiffness using the parameter f. (a) The phase difference Δ_{13} plotted at foot contact of the right hindlimb. The quadruped model adopted the walk, trot, or pace pattern depending on f and the initial state. A gait transition occurs between the walk and trot patterns at different joint stiffnesses depending on the direction of the stiffness change. The pace pattern did not change greatly with f. (b) The footprint diagram for the gait transition from the trot to walk pattern.

from 2.0 or reduced f from 3.2. We examined what gait pattern (represented by Δ_{13}) emerges and how the gait pattern changes with locomotion dynamics.

Figure 5 shows the result obtained when we used the following parameters: $T_{st} = 0.3$ s ($\beta = 0.75$), and $K_{12} = K_{21} = K_{34} = K_{43} = 10$. Figure 5(a) displays the phase difference Δ_{13} when the right hindlimb contacts the ground. When we used a low joint stiffness ($f = 2.0$), the phase difference Δ_{13} converges to a value close to 3.1 or 0.6 rad from various initial values; this implies that trot and pace patterns are respectively produced. On the other hand, when we used a high joint stiffness ($f = 3.2$), the phase difference Δ_{13} converges to a value close to 2.7 or 0.6 rad; this indicates that walk and pace patterns, respectively, are created. (Although $\Delta_{13} = 2.7$ is also close to π, we considered it to indicate the walk pattern to distinguish it from the trot pattern of $\Delta_{13} = 3.1$.)

When we changed the joint stiffness by varying the parameter f, the pace pattern ($\Delta_{13} = 0.6$) did not change greatly, whereas the phase difference Δ_{13} varied from 2.7 to 3.1 rad or from 3.1 to 2.7 rad, indicating that the gait pattern changes between the walk and trot patterns. In particular, when we increased the joint stiffness, the trot pattern changed to the walk pattern around $f = 3.0$ (Fig. 5(b) shows the footprint diagram during this gait transition). In contrast to when the joint stiffness was increased, when we reduced the joint stiffness, the walk pattern changed to the trot pattern at about $f = 2.3$. These results reveal that the gait transition

between the walk and trot patterns occurs at different joint stiffnesses depending on the direction of the stiffness change; that is, the gait pattern transition exhibits hysteresis.

2. Hysteresis by varying the walking speed

In addition to varying the waist joint stiffness, we investigated the effects of varying the walking speed on quadrupedal locomotion dynamics by changing the duty factor β (stance phase duration T_{st}). We used various initial values for the phase difference Δ_{13} with $\beta = 0.745$ or $\beta = 0.756$. After the quadruped model established a steady gait pattern, we slowly increased β from 0.745 or reduced β from 0.756.

Figure 6 shows the result obtained for $f = 2.6$. At a high speed ($\beta = 0.745$), the phase difference Δ_{13} converges to a value close to 3.1 or 0.6 rad from various initial values; this implies that the trot and pace patterns are respectively established. On the other hand, for a low speed ($\beta = 0.756$), the phase difference Δ_{13} converges to a value close to 2.7 or 0.6 rad, indicating that the walk and pace patterns are respectively generated. When we changed the walking speed using the duty factor β, the pace pattern ($\Delta_{13} = 0.6$) did not change greatly, whereas the phase difference Δ_{13} varied from 2.7 to 3.1 rad or from 3.1 to 2.7 rad, implying that the gait pattern changes between the walk and trot patterns. In addition, the gait transition between the walk and trot patterns occurs at different walking speeds depending on the direction of
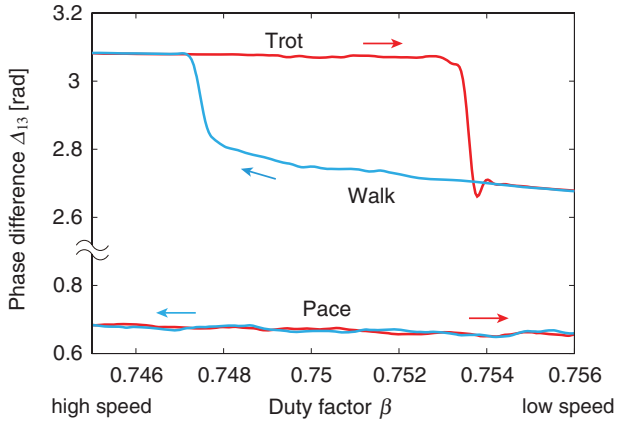
FIG. 6. (Color online) Gait transition induced by changing the walking speed using the duty factor β. This shows the phase relationship between the right forelimb and the right hindlimb Δ_{13}, plotted at the foot contact of the right hindlimb, where the gait transition occurs between the walk and trot patterns at different walking speeds depending on the direction of the speed change.

the speed change; in other words, the gait pattern exhibits hysteresis, similar to when the waist joint stiffness is varied.
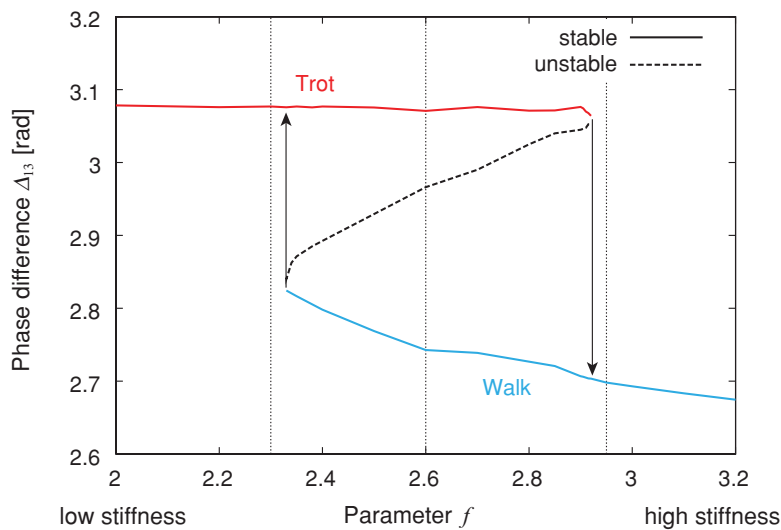
B. Stability characteristics of the hysteresis

The hysteresis in the gait transition between the walk and trot patterns obtained in the previous sections suggests the coexistence of different gait patterns over a range of waist joint stiffnesses and walking speeds. That is, some conditions give rise to more than one attractor. To examine this, we investigated the dynamic characteristics in the hysteresis in the gait transition between the walk and trot patterns when the waist joint stiffness was varied.

Since the gait pattern was determined by one state variable, such as Δ_{13}, as explained in Sec. II D, stability analysis related to Δ_{13} reveals the existence of attractors. Therefore, we used various values of the parameter f and obtained a one-dimensional first return map of the phase difference Δ_{13} for each f by plotting the relationship between the phase difference Δ_{13n} for the nth step and the phase difference Δ_{13n+1} for the next step during locomotion [54,60–62]. We can determine possible gait patterns and their stabilities from the
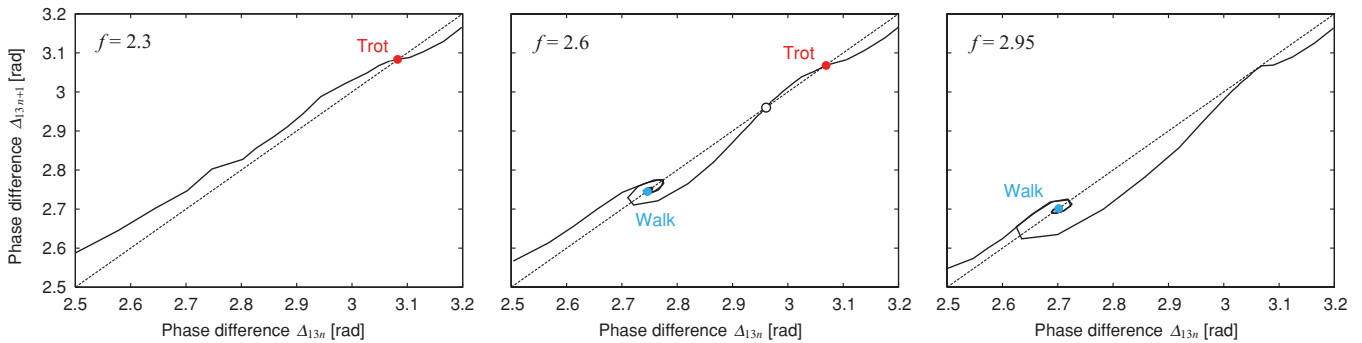
FIG. 7. (Color online) Stability characteristics in the gait patterns. (a) Return maps of the phase difference Δ_{13} for various values of the parameter f by plotting the relationship between phase difference Δ_{13n} for the nth step and phase difference Δ_{13n+1} for the next step during locomotion. Solid and open dots indicate stable and unstable gait patterns, respectively. (b) Stable and unstable gait patterns investigated by the return maps.

intersection of the return map and the diagonal line ($\Delta_{13n+1} = \Delta_{13n}$). From the obtained return maps, we examined the stability relationship between the gait patterns and the waist joint stiffness to investigate the hysteresis mechanism.

Figure 7(a) shows return maps for several values of f. When $f = 2.3$, the return map shows that the trot pattern is the only attractor in this range of the phase difference Δ_{13}. However, when $f = 2.6$, there are two stable gait patterns (trot and walk patterns) and one unstable gait pattern between the stable gait patterns. When $f = 2.95$, the trot pattern disappears due to the loss of the intersections and the walk pattern is the only attractor.

Figure 7(b) shows the stability characteristics obtained from the stable and unstable gait patterns investigated by the return maps. The trot pattern is stable from $f = 2.0$ to 2.92 and the walk pattern is stable from $f = 2.33$ to 3.2. The trot and walk patterns are connected by the unstable gait pattern. The arrows indicate jumps in the waist joint stiffness, which give rise to the hysteresis (jump phenomenon) in the gait pattern. These stability characteristics are also observed when the walking speed is varied.

C. Robustness of the hysteresis for model parameters

We investigated if the hysteresis in the gait transition obtained in the previous sections is specific to the selected model parameters. Specifically, since the mass and size of the bodies are important factors in generating the locomotor behavior, we changed the mass, length, or width of the front and rear bodies and examined if the hysteresis in the gait transition appears and what changes are induced by varying these parameters. Similarly to Sec. III A 1, we changed the waist joint stiffness based on parameter f and investigated how the phase difference Δ_{13} varies.

Figures 8(a)–8(c) show the results obtained when the mass, length, and width of the front and rear bodies were varied, respectively. Although these changes in the physical parameters alter the waist joint stiffness that induces the gait transition between the walk and trot patterns, hysteresis in the gait transition occurs similarly to the previous sections.

IV. DISCUSSION

Our quadruped model consists of a body mechanical system and an oscillator network system. These systems dynamically interact with each other; the oscillator phases in the oscillator network system produce the command signals to create the limb movements and the foot-contact events through the body dynamics modulate the oscillator phases. Physiological studies have revealed that spinal cats create locomotor behaviors on treadmill and their gait pattern changes when the treadmill speed is altered [13,63]. Evidently, the tactile sensory information between their feet and the treadmill belt influences the locomotor phase and rhythm generated by the CPGs [64]. Our simulation results show that a simple dynamic model with interactions among the body mechanical system, the oscillator network system, and the environment based on physiological findings can generate various gait patterns and a gait pattern transition with hysteresis, similar to that observed in animal locomotion.

The gait pattern during locomotion is determined by the phase relationship between the oscillators, which is produced by interactions among the oscillators (6) and phase regulation by phase resetting (7). When we do not use phase resetting, the phase differences Δ_{12} and Δ_{34} converge to π due to the interactions among the oscillators. However, all the values of the phase difference Δ_{13} are neutral and the phase difference Δ_{13} depends only on the initial values of the oscillator phases; it does not depend on the body mechanical system. In addition to this stability structure of the oscillator system, when we incorporated phase resetting, the phase difference Δ_{13} converged to some equilibrium points related to the gait patterns through interactions among the body mechanical system, the oscillator network system, and the environment. In addition, changing the waist joint stiffness and the locomotion speed altered the equilibrium points of the walk and trot patterns and their stabilities.

Our results reveal that the walk pattern is generated at low speeds and the trot pattern is produced at high speeds, which is similar to animal locomotion (Fig. 6). That is, the four
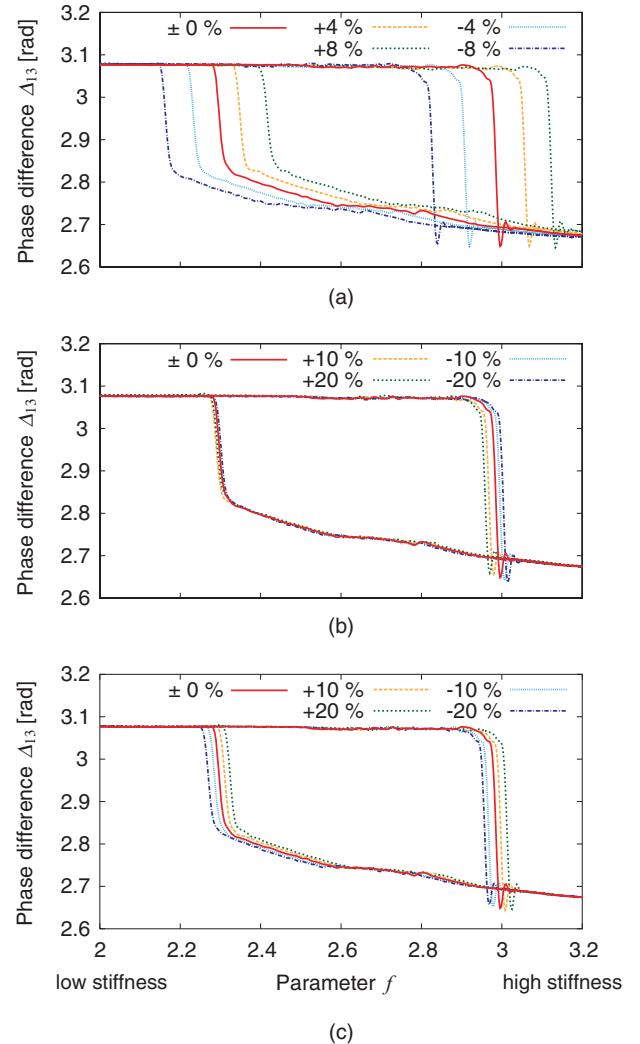

FIG. 8. (Color online) Effects of changing the physical parameters of the quadruped model on the hysteresis in the gait transition induced by changing the waist joint stiffness f. The mass (a), length (b), and width (c) of the front and rear bodies were varied.

limbs are not synchronized at low speeds and two limbs are synchronized at high speeds. Although we used constraints for the phase relationship between the right and left limbs, there were insufficient constraints to fully determine the gait pattern; the gait patterns obtained were generated through the dynamic interactions. Thus the gait patterns are dynamically appropriate for each walking speed. In contrast to the trot and walk patterns, the pace pattern did not change when the physical conditions were varied, implying that it is more stable than the walk and trot patterns. To change the gait pattern from the pace pattern, larger factors for the phase dynamics are required.

Our simulation results reveal that increasing (reducing) the waist joint stiffness and reducing (increasing) the walking speed have similar effects on the gait pattern (Figs. 5 and 6). In addition, changing the physical parameters, such as the mass and the length, alters the waist joint stiffness at which a gait transition occurs (Fig. 8). These results imply that since the joint stiffness and the walking speed respectively influence the natural frequency of the body mechanical system and the frequency of the periodic force induced by the interaction between the feet and the ground, the locomotion dynamics will have similar stability characteristics in relation to changes in these two parameters.

Unlike the walking speed, there is currently no clear experimental evidence showing that gait transitions can be induced by changing the waist joint stiffness in animals. However, the joint stiffness must play an important role in generating locomotor behavior in which coactivation of antagonist muscles affects the joint stiffness [65,66]. In addition to controlling the locomotor phase and rhythm, muscle tone control is important for locomotion since it helps maintain the posture during locomotion [12]. Our results demonstrate that waist joint stiffness plays a similar role in generating various gait patterns and in causing gait pattern transition as the walking speed; this provides meaningful biological insight from the perspective of dynamics.

Hysteresis and jump phenomena are typical characteristics of nonlinear dynamic systems, as observed in the periodically forced Duffing equation [67]. To better understand transition mechanisms in locomotion dynamics, more sophisticated mathematical models should be constructed and experimental investigations using animals and biologically inspired robots in the real world should be performed in the future.

APPENDIX: EQUATION OF MOTION OF BODY MECHANICAL SYSTEM

Here we derive the governing equations for the body mechanical system of our quadruped model. We first derive the equation of motion by assuming that each joint has three rotational degrees of freedom.

To derive the equations, we introduce the following coordinate axes: $\{a_0\} = \{a_{01}\ a_{02}\ a_{03}\}$ is fixed to the ground.

$\{a_{FB}\} = \{a_{FB1}\ a_{FB2}\ a_{FB3}\}$ and $\{a_{RB}\} = \{a_{RB1}\ a_{RB2}\ a_{RB3}\}$ are respectively fixed to the front and rear bodies such that the origin of $\{a_{FB}\}$ is at the center of mass of the front body and the origin of $\{a_{RB}\}$ is at the waist joint. $\{a_{UL}^i\} = \{a_{UL1}^i\ a_{UL2}^i\ a_{UL3}^i\}$ and $\{a_{LL}^i\} = \{a_{LL1}^i\ a_{LL2}^i\ a_{LL3}^i\}$ are fixed in the upper and lower links of limb i ($i = 1, \ldots, 4$), whose origins are at joints 1 and 2 of limb i, respectively. For these coordinate axes, axes denoted by the suffix 1 are in the nominal walking direction, axes with the suffix 2 lie in the lateral direction, and axes with the suffix 3 are vertical when the quadruped model stands with straight limbs.

We introduce the following distance vectors in these coordinate axes: r_{FB} from the center of mass of the front body to the waist joint and r_{FB}^i from the center of mass of the front body to joint 1 of limb i expressed in $\{a_{FB}\}$ ($i = 1,2$); r_{RB}^i from the waist joint to joint 1 of limb i and l_{RB} from the waist joint to the center of mass of the rear body expressed in $\{a_{RB}\}$ ($i = 3,4$); r_{UL}^i from joint 1 to joint 2 and l_{UL}^i from joint 1 to the center of mass of the upper link of limb i expressed in $\{a_{UL}^i\}$ ($i = 1, \ldots, 4$); r_{LL}^i from joint 2 to the limb tip and l_{LL}^i from joint 2 to the center of mass of the lower link of limb i expressed in $\{a_{LL}^i\}$ ($i = 1, \ldots, 4$).

To describe the configuration of the quadruped model, we define the following state vectors in terms of the coordinate axes. $r_0 = [\,x_1\ x_2\ x_3\,]^T$ is the position vector of the center of mass of the front body in $\{a_0\}$. $\theta_{FB} = [\,\theta_1\ \theta_2\ \theta_3\,]^T$ are the Euler angles that express the posture of the front body in $\{a_{FB}\}$. $\theta_{RB,FB} = [\,\theta_{RB,FB1}\ \theta_{RB,FB2}\ \theta_{RB,FB3}\,]^T$ are the Euler angles that indicate the orientations of $\{a_{RB}\}$ relative to $\{a_{FB}\}$. $\theta_{UL,FB}^i = [\,\theta_{UL,FB1}^i\ \theta_{UL,FB2}^i\ \theta_{UL,FB3}^i\,]^T$ are the Euler angles that express the orientations of $\{a_{UL}^i\}$ relative to $\{a_{FB}\}$ ($i = 1,2$). $\theta_{UL,RB}^i = [\,\theta_{UL,RB1}^i\ \theta_{UL,RB2}^i\ \theta_{UL,RB3}^i\,]^T$ are the Euler angles that describe the orientations of $\{a_{UL}^i\}$ relative to $\{a_{RB}\}$ ($i = 3,4$). $\theta_{LL,UL}^i = [\,\theta_{LL,UL1}^i\ \theta_{LL,UL2}^i\ \theta_{LL,UL3}^i\,]^T$ are the Euler angles that indicate the orientations of $\{a_{LL}^i\}$ relative to $\{a_{UL}^i\}$ ($i = 1, \ldots, 4$). ω_{FB} is the angular velocity vector of $\{a_{FB}\}$ relative to $\{a_0\}$ expressed in $\{a_{FB}\}$. $\omega_{RB,FB}$ is the angular velocity vector of $\{a_{RB}\}$ relative to $\{a_{FB}\}$ expressed in $\{a_{RB}\}$. $\omega_{UL,FB}^i$ is the angular velocity vector of $\{a_{UL}^i\}$ relative to $\{a_{FB}\}$ expressed in $\{a_{UL}^i\}$ ($i = 1,2$). $\omega_{UL,RB}^i$ is the angular velocity vector of $\{a_{UL}^i\}$ relative to $\{a_{RB}\}$ expressed in $\{a_{UL}^i\}$ ($i = 3,4$). $\omega_{LL,UL}^i$ is the angular velocity vector of $\{a_{LL}^i\}$ relative to $\{a_{UL}^i\}$ expressed in $\{a_{LL}^i\}$ ($i = 1, \ldots, 4$).

Although we have introduced the Euler angles such that each joint has three rotational degrees of freedom, these Euler angles have the following relationship with the actual joint angles: $\theta_{RB,FB1} = \theta_w$, $\theta_{UL,FB2}^i = \theta_1^i$ ($i = 1,2$), $\theta_{UL,RB2}^i = \theta_1^i$ ($i = 3,4$), and $\theta_{LL,UL2}^i = \theta_2^i$ ($i = 1, \ldots, 4$). Note that the other Euler angles of the joints are constrained after deriving the equations. We employ 3-1-2 Euler angles and introduce coordinate transform matrices $A_{i,j}$ from $\{a_j\}$ to $\{a_i\}$ ($i,j = 0,FB,RB$) and $A_{j,k}^i$ from $\{a_k\}$ to $\{a_j^i\}$ or from $\{a_k^i\}$ to $\{a_j^i\}$ ($i = 1, \ldots, 4$, $j,k = 0,FB,RB,UL,LL$).

We denote state variables $\Theta \in \mathbb{R}^{33}$ and $\Omega \in \mathbb{R}^{33}$ by

$$\Theta = [\,r_0^T\ \theta_{FB}^T\ \theta_{UL,FB}^{1T}\ \theta_{LL,UL}^{1T}\ \theta_{UL,FB}^{2T}\ \theta_{LL,UL}^{2T}$$
$$\theta_{RB,FB}^T\ \theta_{UL,RB}^{3T}\ \theta_{LL,UL}^{3T}\ \theta_{UL,RB}^{4T}\ \theta_{LL,UL}^{4T}\,]^T$$

$$\Omega = \begin{bmatrix} \dot{r}_0^{\mathrm{T}} & \omega_{\mathrm{FB}}^{\mathrm{T}} & \omega_{\mathrm{UL,FB}}^{1\mathrm{T}} & \omega_{\mathrm{LL,UL}}^{1\mathrm{T}} & \omega_{\mathrm{UL,FB}}^{2\mathrm{T}} & \omega_{\mathrm{LL,UL}}^{2\mathrm{T}} \\ & \omega_{\mathrm{RB,FB}}^{\mathrm{T}} & \omega_{\mathrm{UL,RB}}^{3\mathrm{T}} & \omega_{\mathrm{LL,UL}}^{3\mathrm{T}} & \omega_{\mathrm{UL,RB}}^{4\mathrm{T}} & \omega_{\mathrm{LL,UL}}^{4\mathrm{T}} \end{bmatrix}^{\mathrm{T}}. \quad (A1)$$

These variables have the relationship

$$\Omega = \mathcal{B}\dot{\Theta} \tag{A2}$$

where

$$\mathcal{B} = \begin{bmatrix} I & & & & & \\ \hline & B(\theta_{\mathrm{FB}}) & & & & \\ & & \mathcal{B}_{\mathrm{L}}^1 & & & \\ & & & \mathcal{B}_{\mathrm{L}}^2 & & \\ & & & & B(\theta_{\mathrm{RB,FB}}) & \\ & & & & & \mathcal{B}_{\mathrm{L}}^3 \\ & & & & & & \mathcal{B}_{\mathrm{L}}^4 \end{bmatrix}$$
$$\in \mathbb{R}^{33 \times 33}$$

$$\mathcal{B}_{\mathrm{L}}^i = \begin{bmatrix} B(\theta_{\mathrm{UL,FB}}^i) & \\ & B(\theta_{\mathrm{LL,UL}}^i) \end{bmatrix} \in \mathbb{R}^{6 \times 6}, \quad i = 1,2$$

$$\mathcal{B}_{\mathrm{L}}^i = \begin{bmatrix} B(\theta_{\mathrm{UL,RB}}^i) & \\ & B(\theta_{\mathrm{LL,UL}}^i) \end{bmatrix} \in \mathbb{R}^{6 \times 6}, \quad i = 3,4$$

where I is a 3×3 unit matrix and for Euler angles $\psi = [\,\psi_1 \; \psi_2 \; \psi_3\,]^{\mathrm{T}}$, matrix $B(\psi)$ is given by

$$B(\psi) = \begin{bmatrix} \cos\psi_2 & 0 & -\cos\psi_1 \sin\psi_2 \\ 0 & 1 & \sin\psi_1 \\ \sin\psi_2 & 0 & \cos\psi_1 \cos\psi_2 \end{bmatrix}.$$

The kinetic energy ε of this system is given by

$$2\varepsilon = \Omega^{\mathrm{T}}\mathcal{H}^{\mathrm{T}}(\mathcal{L}^{\mathrm{T}}\mathcal{M}\mathcal{L} + \mathcal{J})\mathcal{H}\Omega \tag{A3}$$

where

$$\mathcal{H} =$$

$$\begin{bmatrix} I & & & & & \\ \hline & I & & & & \\ \mathcal{H}_{\mathrm{L,FB}}^1 & & \mathcal{H}_{\mathrm{L,L}}^1 & & & \\ \mathcal{H}_{\mathrm{L,FB}}^2 & & & \mathcal{H}_{\mathrm{L,L}}^2 & & \\ A_{\mathrm{RB,FB}} & & & & I & \\ \mathcal{H}_{\mathrm{L,FB}}^3 & & & & \mathcal{H}_{\mathrm{L,RB}}^3 & \mathcal{H}_{\mathrm{L,L}}^3 \\ \mathcal{H}_{\mathrm{L,FB}}^4 & & & & \mathcal{H}_{\mathrm{L,RB}}^3 & & \mathcal{H}_{\mathrm{L,L}}^4 \end{bmatrix}$$
$$\in \mathbb{R}^{33 \times 33}$$

$$\mathcal{H}_{\mathrm{L,L}}^i = \begin{bmatrix} I & \\ A_{\mathrm{LL,UL}}^i & I \end{bmatrix} \in \mathbb{R}^{6 \times 6}, \quad i = 1,\ldots,4$$

$$\mathcal{H}_{\mathrm{L,FB}}^i = \begin{bmatrix} A_{\mathrm{UL,FB}}^i \\ A_{\mathrm{LL,FB}}^i \end{bmatrix} \in \mathbb{R}^{6 \times 3}, \quad i = 1,\ldots,4$$

$$\mathcal{H}_{\mathrm{L,RB}}^i = \begin{bmatrix} A_{\mathrm{UL,RB}}^i \\ A_{\mathrm{LL,RB}}^i \end{bmatrix} \in \mathbb{R}^{6 \times 3}, \quad i = 3,4$$

$$\mathcal{L} = \mathcal{L}_1 + \mathcal{L}_2$$

$$\mathcal{L}_1 =$$

$$\begin{bmatrix} A_{\mathrm{FB,0}} & O & & \\ \mathcal{L}_{\mathrm{L,0}}^1 & \mathcal{L}_{\mathrm{L,FB}}^1 & \mathcal{L}_{\mathrm{L,L}}^1 & \\ \mathcal{L}_{\mathrm{L,0}}^2 & \mathcal{L}_{\mathrm{L,FB}}^2 & & \mathcal{L}_{\mathrm{L,L}}^2 \\ A_{\mathrm{RB,0}} & A_{\mathrm{RB,FB}}\tilde{r}_{\mathrm{FB}} & O & \\ \mathcal{L}_{\mathrm{L,0}}^3 & \mathcal{L}_{\mathrm{L,FB}}^3 & \mathcal{L}_{\mathrm{L,RB}}^3 & \mathcal{L}_{\mathrm{L,L}}^3 \\ \mathcal{L}_{\mathrm{L,0}}^4 & \mathcal{L}_{\mathrm{L,FB}}^4 & \mathcal{L}_{\mathrm{L,RB}}^3 & \mathcal{L}_{\mathrm{L,L}}^4 \end{bmatrix}$$
$$\in \mathbb{R}^{30 \times 33}$$

$$\mathcal{L}_{\mathrm{L,0}}^i = \begin{bmatrix} A_{\mathrm{UL,0}}^i \\ A_{\mathrm{LL,0}}^i \end{bmatrix} \in \mathbb{R}^{6 \times 3}, \quad i = 1,\ldots,4$$

$$\mathcal{L}_{\mathrm{L,L}}^i = \begin{bmatrix} O & \\ A_{\mathrm{LL,UL}}^i \tilde{r}_{\mathrm{UL}}^i & O \end{bmatrix} \in \mathbb{R}^{6 \times 6}, \quad i = 1,\ldots,4$$

$$\mathcal{L}_{\mathrm{L,FB}}^i = \begin{bmatrix} A_{\mathrm{UL,FB}}^i \tilde{r}_{\mathrm{FB}}^i \\ A_{\mathrm{LL,FB}}^i \tilde{r}_{\mathrm{FB}}^i \end{bmatrix} \in \mathbb{R}^{6 \times 3}, \quad i = 1,2$$

$$\mathcal{L}_{\mathrm{L,FB}}^i = \begin{bmatrix} A_{\mathrm{UL,FB}}^i \tilde{r}_{\mathrm{FB}} \\ A_{\mathrm{LL,FB}}^i \tilde{r}_{\mathrm{FB}} \end{bmatrix} \in \mathbb{R}^{6 \times 3}, \quad i = 3,4$$

$$\mathcal{L}_{\mathrm{L,RB}}^i = \begin{bmatrix} A_{\mathrm{UL,RB}}^i \tilde{r}_{\mathrm{RB}}^i \\ A_{\mathrm{LL,RB}}^i \tilde{r}_{\mathrm{RB}}^i \end{bmatrix} \in \mathbb{R}^{6 \times 3}, \quad i = 3,4$$

$$\mathcal{L}_2 = \begin{bmatrix} & O & & & & \\ & & \mathcal{R}_{\mathrm{L}}^1 & & & \\ \mathcal{O} & & & \mathcal{R}_{\mathrm{L}}^2 & & \\ & & & & \tilde{l}_{\mathrm{RB}} & & \\ & & & & & \mathcal{R}_{\mathrm{L}}^3 & \\ & & & & & & \mathcal{R}_{\mathrm{L}}^4 \end{bmatrix} \in \mathbb{R}^{30 \times 33}$$

$$\mathcal{R}_{\mathrm{L}}^i = \begin{bmatrix} \tilde{l}_{\mathrm{UL}}^i & \\ & \tilde{l}_{\mathrm{LL}}^i \end{bmatrix} \in \mathbb{R}^{6 \times 6}, \quad i = 1,\ldots,4$$

$$\mathcal{M} = \begin{bmatrix} m_{\mathrm{FB}}I & & & & & \\ & \mathcal{M}_{\mathrm{L}}^1 & & & & \\ & & \mathcal{M}_{\mathrm{L}}^2 & & & \\ & & & m_{\mathrm{RB}}I & & \\ & & & & \mathcal{M}_{\mathrm{L}}^3 & \\ & & & & & \mathcal{M}_{\mathrm{L}}^4 \end{bmatrix} \in \mathbb{R}^{30 \times 30}$$

$$\mathcal{M}_{\mathrm{L}}^i = \begin{bmatrix} m_{\mathrm{UL}}^i I & \\ & m_{\mathrm{LL}}^i I \end{bmatrix} \in \mathbb{R}^{6 \times 6}, \quad i = 1,\ldots,4$$

$$\mathcal{J} = \begin{bmatrix} O & & & & & & \\ \hline & J_{\mathrm{FB}} & & & & & \\ & & \mathcal{J}_{\mathrm{L}}^1 & & & & \\ & & & \mathcal{J}_{\mathrm{L}}^2 & & & \\ & & & & J_{\mathrm{RB}} & & \\ & & & & & \mathcal{J}_{\mathrm{L}}^3 & \\ & & & & & & \mathcal{J}_{\mathrm{L}}^4 \end{bmatrix} \in \mathbb{R}^{33 \times 33}$$

$$\mathcal{J}_{\mathrm{L}}^i = \begin{bmatrix} J_{\mathrm{UL}}^i & \\ & J_{\mathrm{LL}}^i \end{bmatrix} \in \mathbb{R}^{6 \times 6}, \quad i = 1, \ldots, 4$$

where O is a 3×3 zero matrix; $\mathcal{O}$ is an appropriately sized zero matrix; m_{FB}, m_{RB}, m_{UL}^i, and m_{LL}^i are the masses of the front body, the rear body, the upper link, and the lower link of limb i ($i = 1, \ldots, 4$); J_{FB}, J_{RB}, J_{UL}^i, and J_{LL}^i are the inertia matrices about the center of mass for the front body, the rear body, the upper link, and the lower link of limb i ($i = 1, \ldots, 4$); and for vector $h = [\, h_1 \ h_2 \ h_3 \,]^{\mathrm{T}}$, matrix $\tilde{h}$ is expressed as

$$\tilde{h} = \begin{bmatrix} 0 & h_3 & -h_2 \\ -h_3 & 0 & h_1 \\ h_2 & -h_1 & 0 \end{bmatrix}.$$

The equation of motion is derived using the Lagrangian equation as

$$\dot{L} + \mathcal{W} L + \mathcal{V} P = G + U + \Gamma, \tag{A4}$$

where $L \in \mathbb{R}^{33}$ is the generalized momentum vector of this system, which is given by $L = \mathcal{H}^{\mathrm{T}}(\mathcal{L}^{\mathrm{T}} \mathcal{M} \mathcal{L} + \mathcal{J}) \mathcal{H} \Omega$, and

$$\mathcal{W} = \begin{bmatrix} O & & & & & & \\ \hline & \tilde{\omega}_{\mathrm{FB}}^{\mathrm{T}} & & & & & \\ & & \mathcal{W}_{\mathrm{L}}^{1\mathrm{T}} & & & & \\ & & & \mathcal{W}_{\mathrm{L}}^{2\mathrm{T}} & & & \\ & & & & \tilde{\omega}_{\mathrm{RB}}^{\mathrm{T}} & & \\ & & & & & \mathcal{W}_{\mathrm{L}}^{3\mathrm{T}} & \\ & & & & & & \mathcal{W}_{\mathrm{L}}^{4\mathrm{T}} \end{bmatrix}$$
$$\in \mathbb{R}^{33 \times 33}$$

$$\mathcal{W}_{\mathrm{L}}^i = \begin{bmatrix} \tilde{\omega}_{\mathrm{UL}}^i & \\ & \tilde{\omega}_{\mathrm{LL}}^i \end{bmatrix} \in \mathbb{R}^{6 \times 6}, \quad i = 1, \ldots, 4$$

$$\begin{bmatrix} \dot{r}_0^{\mathrm{T}} & \omega_{\mathrm{FB}}^{\mathrm{T}} & \omega_{\mathrm{UL}}^{1\mathrm{T}} & \omega_{\mathrm{LL}}^{1\mathrm{T}} & \omega_{\mathrm{UL}}^{2\mathrm{T}} & \omega_{\mathrm{LL}}^{2\mathrm{T}} & \omega_{\mathrm{RB}}^{\mathrm{T}} & \omega_{\mathrm{UL}}^{3\mathrm{T}} & \omega_{\mathrm{LL}}^{3\mathrm{T}} & \omega_{\mathrm{UL}}^{4\mathrm{T}} & \omega_{\mathrm{LL}}^{4\mathrm{T}} \end{bmatrix}^{\mathrm{T}}$$
$$= \mathcal{H} \Omega \in \mathbb{R}^{33}$$

$$\mathcal{V} = \begin{bmatrix} \mathcal{O} & & & & & & \\ \hline \tilde{v}_{\mathrm{FB}}^{\mathrm{T}} & & & & & & \\ & \mathcal{V}_{\mathrm{L}}^{1\mathrm{T}} & & & & & \\ & & \mathcal{V}_{\mathrm{L}}^{2\mathrm{T}} & & & & \\ & & & \tilde{v}_{\mathrm{RB}}^{\mathrm{T}} & & & \\ & & & & \mathcal{V}_{\mathrm{L}}^{3\mathrm{T}} & & \\ & & & & & \mathcal{V}_{\mathrm{L}}^{4\mathrm{T}} & \end{bmatrix} \in \mathbb{R}^{33 \times 30}$$

$$\mathcal{V}_{\mathrm{L}}^i = \begin{bmatrix} \tilde{v}_{\mathrm{UL}}^i & \\ & \tilde{v}_{\mathrm{LL}}^i \end{bmatrix} \in \mathbb{R}^{6 \times 6}, \quad i = 1, \ldots, 4$$

$$\begin{bmatrix} v_{\mathrm{FB}}^{\mathrm{T}} & v_{\mathrm{UL}}^{1\mathrm{T}} & v_{\mathrm{LL}}^{1\mathrm{T}} & v_{\mathrm{UL}}^{2\mathrm{T}} & v_{\mathrm{LL}}^{2\mathrm{T}} & v_{\mathrm{RB}}^{\mathrm{T}} & v_{\mathrm{UL}}^{3\mathrm{T}} & v_{\mathrm{LL}}^{3\mathrm{T}} & v_{\mathrm{UL}}^{4\mathrm{T}} & v_{\mathrm{LL}}^{4\mathrm{T}} \end{bmatrix}^{\mathrm{T}}$$
$$= \mathcal{L}_1 \mathcal{H} \Omega \in \mathbb{R}^{30}$$

$$P = \hat{\mathcal{H}}^{\mathrm{T}} \mathcal{M} \mathcal{L} \mathcal{H} \Omega \in \mathbb{R}^{30}, \quad \mathcal{H} = \begin{bmatrix} I & \\ \hline & \hat{\mathcal{H}} \end{bmatrix}$$

and $G \in \mathbb{R}^{33}$ is the gravity term, $U \in \mathbb{R}^{33}$ is the joint torque term, and $\Gamma \in \mathbb{R}^{33}$ is the ground reaction force term, which are derived below. The gravity term G is given by

$$G = \mathcal{H}^{\mathrm{T}} \mathcal{L}^{\mathrm{T}} \mathcal{M} \mathcal{F} g \tag{A5}$$

where

$$\mathcal{F} = \begin{bmatrix} A_{\mathrm{FB},0} \\ \mathcal{F}_{\mathrm{L}}^1 \\ \mathcal{F}_{\mathrm{L}}^2 \\ A_{\mathrm{RB},0} \\ \mathcal{F}_{\mathrm{L}}^3 \\ \mathcal{F}_{\mathrm{L}}^4 \end{bmatrix} \in \mathbb{R}^{30 \times 3}$$

$$\mathcal{F}_{\mathrm{L}}^i = \begin{bmatrix} A_{\mathrm{UL},0}^i \\ A_{\mathrm{LL},0}^i \end{bmatrix} \in \mathbb{R}^{6 \times 3}, \quad i = 1, \ldots, 4$$

$$g = [\, 0 \ 0 \ -g_0 \,]^{\mathrm{T}}$$

and g_0 is the acceleration due to gravity. The joint torque term U is expressed by

$$U = \begin{bmatrix} \overbrace{0 \cdots 0}^{6} & u_{\mathrm{UL}}^{1\mathrm{T}} & u_{\mathrm{LL}}^{1\mathrm{T}} & u_{\mathrm{UL}}^{2\mathrm{T}} & u_{\mathrm{LL}}^{2\mathrm{T}} & u_{\mathrm{RB}}^{\mathrm{T}} & u_{\mathrm{UL}}^{3\mathrm{T}} & u_{\mathrm{LL}}^{3\mathrm{T}} & u_{\mathrm{UL}}^{4\mathrm{T}} & u_{\mathrm{LL}}^{4\mathrm{T}} \end{bmatrix}^{\mathrm{T}}$$

where $u_{\mathrm{RB}} = [\, u_{\mathrm{RB1}} \ u_{\mathrm{RB2}} \ u_{\mathrm{RB3}} \,]^{\mathrm{T}}$, $u_{\mathrm{UL}}^i = [\, u_{\mathrm{UL1}}^i \ u_{\mathrm{UL2}}^i \ u_{\mathrm{UL3}}^i \,]^{\mathrm{T}}$, and $u_{\mathrm{LL}}^i = [\, u_{\mathrm{LL1}}^i \ u_{\mathrm{LL2}}^i \ u_{\mathrm{LL3}}^i \,]^{\mathrm{T}}$ ($i = 1, \ldots, 4$) have the following relation with the actual joint torques: $u_{\mathrm{RB1}} = u_{\mathrm{w}}$, $u_{\mathrm{UL1}}^i = u_1^i$, $u_{\mathrm{LL2}}^i = u_2^i$ ($i = 1, \ldots, 4$), and the other torques are set to 0, where u_{w}, u_1^i, and u_2^i ($i = 1, \ldots, 4$) are the torques at the waist joint and joints 1 and 2 of limb i, respectively. In particular, since the waist joint moves passively based on a torsional spring and damper system, u_{w} is given by

$$u_{\mathrm{w}} = -\kappa_{\mathrm{w}} \theta_{\mathrm{w}} - \sigma_{\mathrm{w}} \dot{\theta}_{\mathrm{w}}, \tag{A6}$$

where κ_{w} and σ_{w} are the spring and damping constants, respectively. The ground reaction force term Γ is derived as

follows. First, the position vector $r_{TL}^i = [r_{TL1}^i \; r_{TL2}^i \; r_{TL3}^i]^T$ of the tip of limb i ($i = 1, \ldots, 4$) is expressed in terms of $\{a_0\}$ as

$$r_{TL}^i = \begin{cases} r_0 + A_{FB,0}^T r_{FB} + A_{UL,0}^{iT} r_{UL}^i + A_{LL,0}^{iT} r_{LL}^i \\ \qquad\qquad\qquad\qquad\qquad\qquad\quad i = 1,2 \\ r_0 + A_{FB,0}^T r_{FB} + A_{RB,0}^T r_{RB}^i + A_{UL,0}^{iT} r_{UL}^i \\ \quad + A_{LL,0}^{iT} r_{LL}^i \qquad\qquad\qquad i = 3,4 \end{cases} \quad (A7)$$

When the limb tip is in contact with the ground, it is constrained by the ground and experiences a reaction force from the ground. We model the ground reaction force $\lambda^i = [\lambda_1^i \; \lambda_2^i \; \lambda_3^i]^T$ of limb i ($i = 1, \ldots, 4$) expressed in $\{a_0\}$ using viscoelastic elements given by

$$\lambda^i = \begin{cases} -K_{TL}(r_{TL}^i - r_{TL}^{i*}) - D_{TL}\dot{r}_{TL}^i & r_{TL3}^i \leqslant 0 \\ 0 & r_{TL3}^i > 0 \end{cases} \\ \qquad\qquad\qquad\qquad\qquad\qquad\qquad i = 1, \ldots, 4, \quad (A8)$$

where r_{TL}^{i*} is the position vector on which the tip of limb i is constrained ($i = 1, \ldots, 4$), and $K_{TL} = \text{diag}(\kappa_{TL1}, \kappa_{TL2}, \kappa_{TL3})$

and $D_{TL} = \text{diag}(\sigma_{TL1}, \sigma_{TL2}, \sigma_{TL3})$ are viscoelastic parameters. The ground reaction force term Γ is then given by

$$\Gamma = (\mathcal{E}^T \mathcal{B}^{-1})^T \Lambda, \quad (A9)$$

where

$$\mathcal{E}^T = \frac{\partial R_{TL}}{\partial \Theta} \in \mathbb{R}^{12 \times 33}$$

$$R_{TL} = [r_{TL}^{1T} \; r_{TL}^{2T} \; r_{TL}^{3T} \; r_{TL}^{4T}]^T \in \mathbb{R}^{12}$$

$$\Lambda = [\lambda^{1T} \; \lambda^{2T} \; \lambda^{3T} \; \lambda^{4T}]^T \in \mathbb{R}^{12}.$$

Finally, redundant angles are contracted since each joint of our model has only one degree of freedom. We obtain the equation of motion for our model (1) by setting the redundant angles (i.e., the Euler angles that are not required to specify the actual joint angles) to zero and eliminating the rows and columns of the matrices and the components of the vectors in the equation of motion (A4) that correspond to these redundant angles.

[1] F. Diedrich and W. Warren, J. Exp. Psychol. Hum. Percept. Perform. **21**, 183 (1995).

[2] T. Griffin, R. Kram, S. Wickler, and D. Hoyt, J. Exp. Biol. **207**, 4215 (2004).

[3] N. Heglund and C. Taylor, J. Exp. Biol. **138**, 301 (1998).

[4] A. Hreljac, R. Imamura, R. Escamilla, and W. Edwards, Gait Posture **25**, 419 (2007).

[5] C. Lamoth, A. Daffertshofer, R. Huys, and P. Beek, Hum. Mov. Sci. **28**, 371 (2009).

[6] A. Raynor, C. Yi, B. Abernethy, and Q. Jong, Hum. Mov. Sci. **21**, 785 (2002).

[7] V. Segers, P. Aerts, M. Lenoir, and D. Clercq, Gait Posture **24**, 247 (2006).

[8] M. Turvey, K. Holt, M. LaFlandra, and S. Fonseca, J. Motor Behav. **31**, 265 (1999).

[9] D. Hoyt and C. Taylor, Nature **292**, 239 (1981).

[10] C. Farley and C. Taylor, Science **253**, 306 (1991).

[11] S. Grillner, Nat. Rev. Neurosci. **4**, 573 (2003).

[12] S. Mori, Prog. Neurobiol. **28**, 161 (1987).

[13] G. Orlovsky, T. Deliagina, and S. Grillner, *Neuronal Control of Locomotion: From Mollusc to Man* (Oxford University Press, 1999).

[14] M. Shik and G. Orlovsky, Phys. Rev. **56**, 465 (1976).

[15] C. Canavier, R. Butera, R. Dror, D. Baxter, J. Clark, and J. Byrne, Biol. Cybern. **77**, 367 (1997).

[16] M. Golubitsky, I. Stewart, P. Buono, and J. Collins, Physica D **115**, 56 (1998).

[17] M. Golubitsky, I. Stewart, P. Buono, and J. Collins, Nature **401**, 693 (1999).

[18] S. Ito, H. Yuasa, Z. Luo, M. Ito, and D. Yanagihara, Biol. Cybern. **78**, 337 (1998).

[19] G. Schtner, W. Jiang, and J. Kelso, J. Theor. Biol. **142**, 359 (1990).

[20] R. Alexander, Philos. Trans. R. Soc. London B **338**, 189 (1992).

[21] S. Aoi, N. Ogihara, T. Funato, Y. Sugimoto, and K. Tsuchiya, Biol. Cybern. **102**, 373 (2010).

[22] H. Geyer, A. Seyfarth, and R. Blickhan, Proc. R. Soc. London, Ser. B **273**, 2861 (2006).

[23] V. B. Kokshenev, Phys. Rev. Lett. **93**, 208101 (2004).

[24] K. Ohgane and K. I. Ueda, Phys. Rev. E **77**, 051915 (2008).

[25] K. Ohgane and K. I. Ueda, Phys. Rev. E **81**, 041909 (2010).

[26] M. Srinivasan and A. Ruina, Nature **439**, 72 (2006).

[27] G. Taga, Physica D **75**, 190 (1994).

[28] B. J. West and N. Scafetta, Phys. Rev. E **67**, 051917 (2003).

[29] P. Holmes, R. Full, D. Koditschek, and J. Guckenheimer, SIAM Rev. **48**, 207 (2006).

[30] A. Ijspeert, A. Crespi, D. Ryczko, and J. Cabelguen, Science **315**, 1416 (2007).

[31] A. Ijspeert, Neural Networks **21**, 642 (2008).

[32] J. Schmitt and P. Holmes, Physica D **156**, 139 (2001).

[33] S. Steingrube, M. Timme, F. Wörgötter, and P. Manoonpong, Nat. Phys. **6**, 224 (2010).

[34] K. Tsujita, K. Tsuchiya, and A. Onat, in *Proceedings of IEEE/RSJ International Conference on Intelligent Robots and Systems*, (IEEE, Maui, USA, 2001), pp. 2318–2325.

[35] H. Kimura, Y. Fukuoka, and A. Cohen, Int. J. Robot. Res. **26**, 475 (2007).

[36] P. Guertin, Brain Res. Rev. **62**, 45 (2009).

[37] D. McCrea and I. Rybak, Brain Res. Rev. **57**, 134 (2008).

[38] R. Burke, A. Degtyarenko, and E. Simon, J. Neurophysiol. **86**, 447 (2001).

[39] M. Lafreniere-Roula and D. McCrea, J. Neurophysiol. **94**, 1120 (2005).

[40] I. Rybak, N. Shevtsova, M. Lafreniere-Roula, and D. McCrea, J. Physiol. **577**, 617 (2006).

[41] I. Rybak, K. Stecina, N. Shevtsova, and D. McCrea, J. Physiol. **577**, 641 (2006).

[42] G. Bosco and R. Poppele, Physiol. Rev. **81**, 539 (2001).

[43] R. Poppele, G. Bosco, and A. Rankin, J. Neurophysiol. **87**, 409 (2002).

[44] R. Poppele and G. Bosco, Trends Neurosci. **26**, 269 (2003).

[45] G. Goslow Jr., R. Reinking, and D. Stuart, J. Morphol. **141**, 1 (1973).

[46] M. Hoy and R. Zernicke, J. Biomech. **18**, 49 (1985).

[47] I. Aihara, Phys. Rev. E **80**, 011918 (2009).

[48] T. Aoyagi and M. Nomura, Phys. Rev. Lett. **83**, 1062 (1999).

[49] T. Aoki and T. Aoyagi, Phys. Rev. Lett. **102**, 034101 (2009).

[50] T. Ichinomiya, Phys. Rev. E **70**, 026116 (2004).

[51] I. Kiss, Y. Zhai, and J. Hudson, Science **296**, 1676 (2002).

[52] H. Kori, Y. Kawamura, H. Nakao, K. Arai, and Y. Kuramoto, Phys. Rev. E **80**, 036207 (2009).

[53] Y. Kuramoto, *Chemical Oscillations, Waves, and Turbulence* (Springer-Verlag, New York, 1984).

[54] N. Nakagawa and Y. Kuramoto, Prog. Theor. Phys. **89**, 313 (1993).

[55] S. Strogatz, D. Abrams, A. McRobie, B. Eckhardt, and E. Ott, Nature **438**, 43 (2005).

[56] B. Conway, H. Hultborn, and O. Kiehn, Exp. Brain Res. **68**, 643 (1987).

[57] J. Duysens, Brain Res. **133**, 190 (1977).

[58] T. Nomura, K. Kawa, Y. Suzuki, M. Nakanishi, and T. Yamasaki, Chaos **19**, 026103 (2009).

[59] S. Aoi, H. Sasaki, and K. Tsuchiya, SIAM J. Appl. Dyn. Syst. **6**, 348 (2007).

[60] D. J. Christini and J. J. Collins, Phys. Rev. Lett. **75**, 2782 (1995).

[61] R. May, Nature **261**, 459 (1976).

[62] S. Schiff, K. Jerger, D. Duong, T. Chang, M. Spano, and W. Ditto, Nature **370**, 615 (1994).

[63] H. Forssberg and S. Grillner, Brain Res. **50**, 184 (1973).

[64] J. Duysens, F. Clarac, and H. Cruse, Physiol. Rev. **80**, 83 (2000).

[65] S. Hagood, M. Solomonow, R. Baratta, B. Zhou, and R. D'Ambrosia, Am. J. Sports Med. **18**, 182 (1990).

[66] D. R. Humphrey and D. J. Reed, in *Motor control mechanisms in health and disease* edited by J. E. Desmedt (Raven Press, New York, 1983), pp. 347–372.

[67] P. Holmes and D. Rand, J. Sound Vib. **44**, 237 (1976).